Dynamics of triple-flames in ignition of turbulent dual fuel mixture: a direct numerical simulation study

Tai Jin[1,2], Kai H. Luo[2], Xujiang Wang[2], Kun Luo[1*], Jianren Fan[1]

1. State Key Laboratory of Clean Energy Utilization, Zhejiang University, Hangzhou 310027, P. R. China
2. Department of Mechanical Engineering, University College London, London WC1E 7JE, United Kingdom

*Corresponding author E-mail: zjulk@zju.edu.cn

This paper is prepared for the colloquium of **Internal Combustion Engines** of the 37th International Symposium on Combustion. Supplemental materials are provided for better understanding of this manuscript.

The total length of the paper is **5786 words** and the Method 1 (M1) is adopted.

Main Text: 3043 words

Fig. 1: (71.6 mm+10 mm)*2.2 words/mm*1+11= 191 words

Fig. 2: (110 mm+10 mm)*2.2 words/mm*2+70 = 598 words

Fig. 3: (58.9 mm+10 mm)*2.2 words/mm*1+40= 192 words

Fig. 4: (42.6 mm+10 mm)*2.2 words/mm*1+57= 172 words

Fig. 5: (93.2 mm+10 mm)*2.2 words/mm*2+24= 478 words

Fig. 6: (43.2 mm+10 mm)*2.2 words/mm*2+30= 264 words

Fig. 7: (33.6 mm+10 mm)*2.2 words/mm*2+39= 231 words

Equation: (1 line +2 line)*7.6 words/line*1= 23 words

References: (32+2)*2.3*7.6 = 594 words

Total = **5786 words**

Payment will be made for colour figures in print.

Abstract: Pilot-ignited dual fuel combustion involves a complex transition between the pilot fuel autoignition and the premixed-like phase of combustion, which is challenging for experimental measurement and numerical modelling, and not sufficiently explored. To further understand the fundamentals of the dual fuel ignition processes, the transient ignition and subsequent flame development in a turbulent dimethyl ether (DME)/methane-air mixing layer under diesel engine-relevant conditions are studied by direct numerical simulations (DNS). Results indicate that combustion is initiated by a two-stage autoignition that involves both low-temperature and high-temperature chemistry. The first stage autoignition is initiated at the stoichiometric mixture, and then the ignition front propagates against the mixture fraction gradient into rich mixtures and eventually forms a diffusively-supported cool flame. The second stage ignition kernels are spatially distributed around the most reactive mixture fraction with a low scalar dissipation rate. Multiple triple flames are established and propagate along the stoichiometric mixture, which is proven to play an essential role in the flame developing process. The edge flames gradually get close to each other with their branches eventually connected. It is the leading lean premixed branch that initiates the steady propagating methane-air flame. The time required for steady flame propagation is substantially shorter than the autoignition delay time of the methane-air mixture under the same thermochemical condition. Temporal evolution of the displacement speed at the flame front is also investigated to clarify the propagation characteristics of the combustion waves. Cool flame and propagation of triple flames are also identified in this study, which are novel features of the pilot-ignited dual fuel combustion.

Keywords: dual-fuel combustion, autoignition, low-temperature combustion, triple flame, direct numerical simulation

1. Introduction

The concept of dual-fuel combustion systems has been explored both on reciprocating engines with emphasis on pollutant emission [1-3] and on staged gas turbine combustors, in which different fuels may be injected in sequential chambers [4]. Previous studies have mostly focused on global quantities, such as engine power output and emission levels [5-7]. Recently, several fundamental experiments have been conducted to investigate dual-fuel flame structures [8, 9]. Despite these efforts, the ignition and flame development processes occurring in such a dual-fuel mixture have not been studied in sufficient details from a fundamental perspective.

Pilot-ignited dual fuel combustion usually involves combined processes of autoignition, diffusion flames, and flame propagation, which is challenging for experimental measurement and numerical modelling [10, 11]. Various numerical models have been developed for dual fuel engine modelling, such as phenomenological approaches [12], quasi-two zone up to multi-zone models [13, 14], and level-set G-equation approach coupled with Shell Ignition and Characteristic-Time-Combustion (CTC) models [15]. Recently, turbulent combustion models with detailed chemistry have been extended to dual-fuel combustion simulations. A two-dimensional unsteady flamelet model was proposed by Doran et al. [16] for modelling ignition in multi-feed combustion systems. Schlatter et al. [17] used a two-dimension Conditional Moment Closure (CMC) formulation and defined the hot spots predicted from the CMC model as the initial kernels of a premixed flame. Soriano et al. [18] developed a hybrid two-dimensional CMC and level-set G-equation model, to account for the autoignition and the subsequent flame propagation, respectively. The flame structures were explored in a conditioning-variable space, while the transient development and the underlying mechanism inducing the premixed flame initiation needs further investigations.

Direct numerical simulations (DNS) of ignition and flame propagation under turbulent conditions has been proved to be a valuable scientific tool for understanding the effects of turbulent mixing and aerodynamic straining on the initial ignition and the subsequent turbulent flame propagation [10, 11, 19-21]. Wang et al. [10] conducted computations of flame development in laminar n-heptane/methane-

air mixing layers. The pressure, temperature and equivalence ratio of the homogeneous mixture as well as the mixing layer thickness were varied to study their effects on the flame development process, in particular the characteristic time required for steady flame propagation. Demosthenous et al. [11] conducted DNS of premixed methane flame initiation by pilot n-heptane spray autoignition. It was found that the n-heptane kernels acted as the source of ignition for the premixed methane flame. They also reported DNS of autoignition in turbulent methane-air mixing layers with n-heptane droplets added [21]. Yao et al. performed DNS of turbulent hydrogen-air mixing layers at pressures up to 30 atm [].

A two-stage autoignition under diesel engine-relevant conditions has been observed [22], involving pre-ignition reactions due to low-temperature chemistry (LTC), followed by the main ignition due to high-temperature chemistry (HTC), which is associated with the "negative temperature coefficient" (NTC). Borghesi et al. [23] conducted a DNS study of autoignition of a sparse spray of n-heptane at 24 bar with reduced chemistry. The doubly conditioned statistics revealed a two-stage autoignition. Krisman et al. [24, 25] recently investigated the two-stage ignition in a turbulent mixing layer of dimethyl ether (DME)-air mixture by DNS. It was found that LTC can strongly affect the timing and location of the second stage autoignition. A further 3D DNS of a temporally evolving planar jet of n-heptane in high temperature air has also been conducted with global chemistry [26].

The NTC effects would make the dual-fuel ignition problem even more complicated. In the present work, DNS is performed to investigate ignition and flame development in turbulent dual-fuel mixtures under diesel engine-relevant conditions. DME is employed as the ignition trigger. The methane-air mixture is considered as homogeneous and forms a mixing layer with DME. The objectives of this work are to scrutinize the premixed methane flame initiation process with pilot DME, and to investigate the role of triple flames therein. The data can also serve as a benchmark for development and validation of various ignition models for pilot-ignited dual-fuel combustion.

2. Numerical methods and initial conditions

Turbulent reacting flows are governed by the continuity equation, the Navier-Stokes equations, and transport equations for species and energy. The solver is a fully compressible in-house DNS code, which has been well validated through simulations of laboratory scale turbulent jet flames and employed for various combustion processes [27, 28]. All spatial derivatives are discretized with eighth-order central differencing schemes, along with a tenth-order filter to remove spurious high frequency fluctuations. The time integration is advanced with an explicit fourth-order Runge-Kutta method. A reduced chemical mechanism consisting of 25 species and 147 reaction steps for oxidation of DME/methane-air mixtures has been developed from the detailed chemical kinetic model (Mech_56.54) of Burke et al. [29], by using the quasi steady state approximations (QSSA) [30]. The reduced mechanism has been validated for ignition delay times and laminar flame speed at conditions relevant to the current study (not shown due to space limit). The mixture is assumed to be an ideal gas. All thermodynamic and transport properties for the individual species and the averaged mixture are calculated based on the Chemkin software libraries [31].

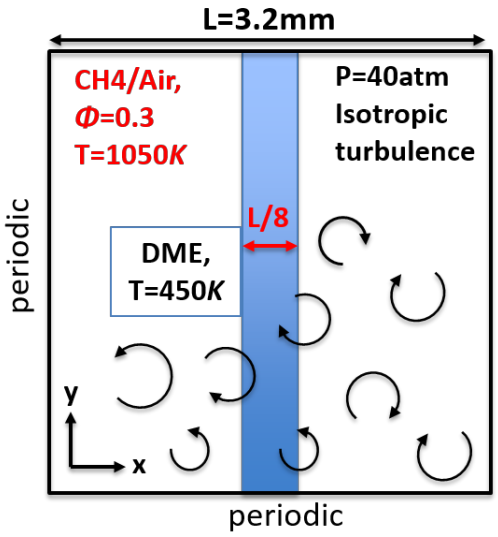

Fig. 1. The computational domain with DME and homogeneous methane-air mixture.

The computational domain is initialized with a slab of pure DME in high temperature homogenous mixture of methane and air at an equivalence ratio of 0.3, as illustrated in **Fig. 1**. The square domain has a size of 3.2 mm by 3.2 mm (L). The 2D configuration is considered here as 3D simulations were still not feasible as discussed in [25]. Periodic boundary conditions were imposed in all directions such that combustion occurs in constant volume. The slab of fuel is initiated in the centre with a width of

L/8 and a temperature of 450K. The system has an initial pressure of 40 atm, and the temperature of the premixed methane-air mixture is 1050 K. The initial composition and temperature vary across the DME/methane-air mixing layer with a specified hyperbolic tangent profile, defined as: $f(x) = \left(\frac{f_1+f_2}{2}\right) + \left(\frac{f_1-f_2}{2}\right)\tanh\left(abs(\frac{x-x_c}{\delta})\right)$, where $f(x)$ is a general parameter which can represent the mass fraction of DME or temperature *T* as a function of *x*. x_c represents half width of the fuel slab. δ is the initial thickness of the mixing layer with a value of 40 μm. Initial methane and air profiles are set according to the mixing line while all other species are initially set to zero. The initial mean flow velocity is set to be zero, and the initial turbulent flow field is generated using an isotropic kinetic energy spectrum function by Passot-Pouquet [32]: $E(k) = \frac{32}{3}\sqrt{\frac{2}{\pi}}\frac{u'^2}{k_e}\left(\frac{k}{k_e}\right)^4 exp\left[-2\left(\frac{k}{k_e}\right)^2\right]$, where k is the wave number, the subscript e stands for the most energetic wave number, and u' is the root mean square (RMS) velocity. The integral length scale l_t of the prescribed turbulence equals 0.2 mm, while the initial root mean square turbulent velocity fluctuation u' is set to be 0.5 m/s. The corresponding Damkhöler numbers (*Da*, defined as $Da=\tau_{turb}/\tau_{ign}$) is about 1.0. τ_{turb} is the large eddy time defined as $\tau_{turb}=l_t/u'$. τ_{ign} is the ignition delay time of the second stage ignition measured in a 1D mixing layer under the same thermochemical condition, as detailed in the **supplementary material**. Similar with a previous DNS of ignitions in turbulent DME/air mixing layer [25], a uniform mesh with resolution of 1μm in both directions is applied to resolve the very thin flame under high pressure conditions, and a time step of 1 ns is used.

3. Results and discussions

3.1 Autoignition and flame development

A typical sequence of the ignition process is illustrated by the temporal evolution of heat release rate (HRR) in **Fig. 2**. The mixture fraction ξ is defined based on the nitrogen mass fraction, ranging between 0 in the methane/air premixed mixture and 1 in the pilot DME [11]. The first stage autoignition is initiated around the ξ_{st} mixture as shown in **Fig. 2(a)**, and then the ignition front propagates up the mixture fraction gradient into richer mixtures as a diffusively-supported cool flame

in **Fig. 2(c)**. The second stage ignition kernels are spatially distributed in rich mixtures around the most reactive mixture fraction $\xi_{mr,1d}$, which is represented by a solid black line as shown in **Fig. 2(d)**. Here, $\xi_{mr,1d}$ corresponds to the second stage ignition of the corresponding 1D mixing layer and equals 0.241 as detailed in the **supplementary material**.

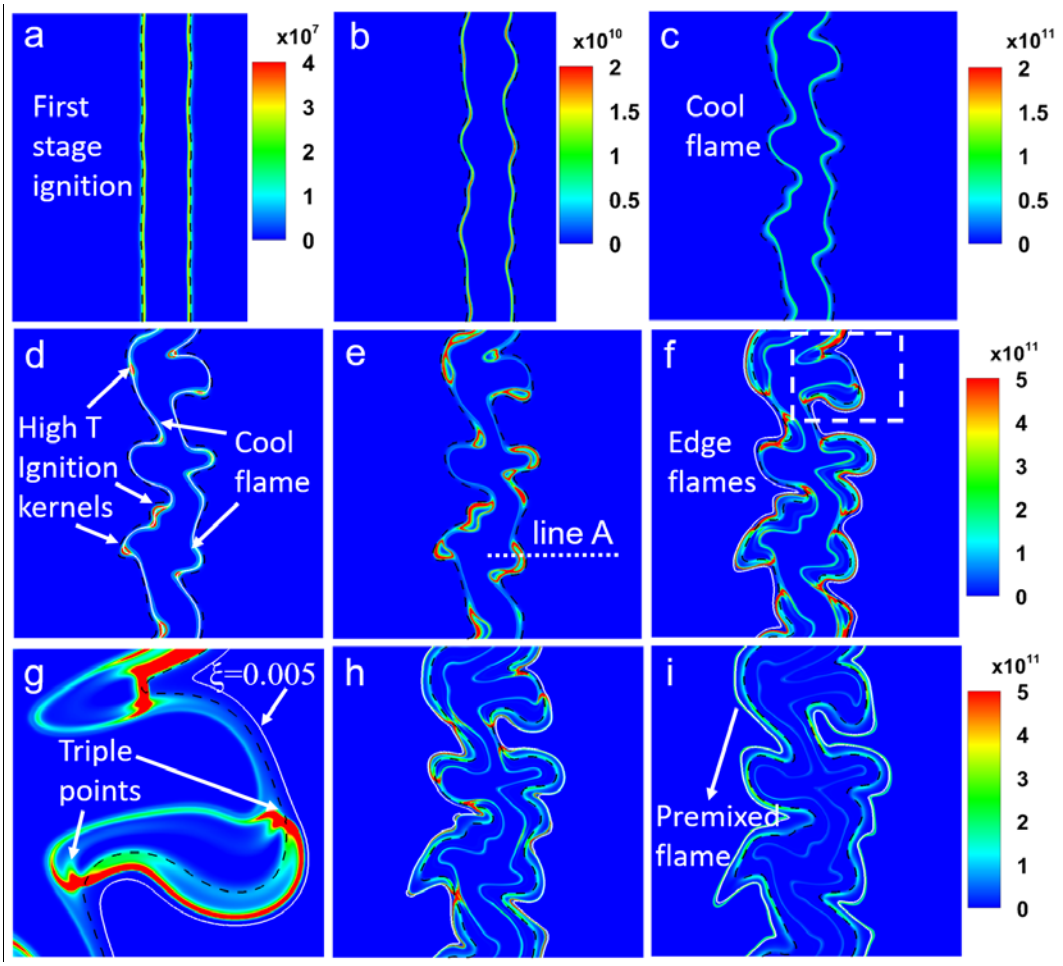

Fig. 2. Temporal evolution of heat release rate (W/m^3). The black dashed line is the ξ_{st} surface, the white solid line in (d) is the $\xi_{mr,1d}$ surface, the white solid lines in (f-i) are the ξ=0.005 surface, which approximately demonstrate the premixed methane-air mixture. (g) is a regional zoomed part of (f). The corresponding instants of (a-i) are 0.008, 0.06, 0.16, 0.23, 0.25, 0.29, 0.29, 0.33 and 0.41 ms, respectively.

The high temperature ignition kernels quickly expand both to richer mixture which collides with the cool flame, and to leaner mixture till they penetrate the stoichiometric mixture isoline, as shown in **Fig. 2(e)**. Thereafter, edge flames are formed and propagate into a partially reacted mixture with opposite directions along the ξ_{st} surface in **Fig. 2(f)**. Note here that the stoichiometric composition is determined by the sum of DME and methane-air mixture. The edge flames include a main tribrachial (triple) flame composed of leading lean and rich premixed branches, and a trailing nonpremixed branch,

which emerge at the triple point, as zoomed in **Fig. 2(g)**. The cool flame can be considered as a fourth branch of the edge-flames, resembling the tetrabrachial flames as observed before under similar thermochemical conditions in the DME-air mixing layer [24, 25]. The edge flames gradually collide with each other and their branches are eventually connected. Meanwhile, the leading lean premixed branches propagate into the premixed methane-air mixture, which can be approximately demonstrated by the ξ=0.005 surface as shown in **Figs. 2(f-i)**. These branches finally trigger the premixed methane-air flame, with a lower heat release rate as shown in **Figs. 2(h) and (i)**. The flame front propagating along line A in **Fig. 2(e)**, as an example, will be further analysed in Section 3.3.

Overall, it can be found that the flame initiation dynamics in the studied pilot-ignited dual fuel combustion are complicated, involving both low- and high-temperature autoignition, cool flames, propagation and collision of triple flames, and transition to a propagating premixed methane-air flame. Low-temperature ignition is initiated around the stoichiometric mixture and then rapidly move to rich mixtures. High-temperature ignition kernels preferably occur at distributed locations around a most reaction mixture. The exact locations of kernel formation are important for the overall ignition and stabilization process, and also important for the conceptual models of diesel-methane dual fuel combustion. Multiple ignition kernels sequentially appear and gradually transit to triple flames. These results demonstrate that propagation and collision of triple flames play an essential role during the flame developing process, and it is the leading lean premixed branches of the triple flames that initiate the steady propagating methane-air flame.

3.2 Ignition and propagation in mixture fraction space

Scalar dissipation rate χ has been proven to significantly influence autoignition. Turbulent mixing induces a wide range of scalar dissipation rate χ. High χ values result in low heat release rate and even the absence of ignition [33]. The doubly conditioned heat release rate (HRR) during the ignition process at several time instants are plotted in **Fig. 3**. The samples of χ values are divided into four levels according to its probability $F(\chi) = F_{\chi|\xi}(\bar{\chi}|\eta)$: low ($\bar{\chi}|F(\chi) < 0.2$); moderate ($\bar{\chi}|0.2 < F(\chi) < 0.5$); high ($\bar{\chi}|0.5 < F(\chi) < 0.8$); and intense ($\bar{\chi}|F(\chi) > 0.8$) [34]. The initial scalar gradient induces

a moderate level of χ, thus the first stage autoignition occurs in a continuous region, other than the localised "spotty" pattern observed in [25]. The LTC transitions to a diffusively-supported cool flame, moving up the mixture fraction gradient into the rich mixture. The mixture fraction corresponding to the peak heat release increases gradually from **Figs. 3(a) to (c)**, while the peak heat release first increases from **Figs. 3(a) to (b)** and then decreases in **Figs. 3(c)**. Turbulence modifies the initial scalar gradient and generates a range of χ, while low χ favours ignition. As shown in **Fig. 3 (c) & (d)**, the second stage ignition with rather high HRR occurs at low scalar dissipation rate χ around $\xi_{mr,1d}$=0.241. Another peak of HRR in the rich mixture (ξ≈0.54) with high χ corresponds to the cool flame.

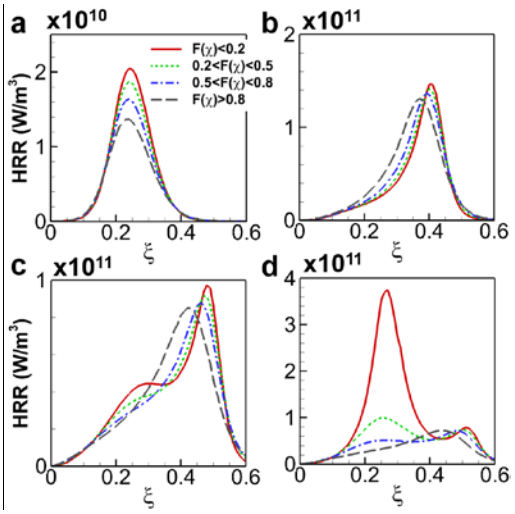

Fig. 3. Doubly conditioned heat release rate (HRR) on mixture fraction ξ and the indicated scalar dissipation rate range χ, (a) t = 0.06 ms, (b) t = 0.12 ms, (c) t = 0.18 ms, (d) t = 0.22 ms

The role of diffusion in supporting the cool flame can be quantified by considering the transport budget analysis for the LTC marker $Y_{CH3OCH2O2}$ [25]. **Figure 4** shows reaction and diffusion terms of the transport budget of $Y_{CH3OCH2O2}$ in addition to χ evaluated along line A at different time instants. It is found that autoignition occurs at relatively low χ, where the magnitude of the reaction term is significantly larger than the diffusion term during ignition. As time advances, both the reaction and diffusion terms increase, while χ gradually decreases. Finally, at t = 0.2 ms in **Fig. 4(d)**, the reaction and diffusion terms have comparable magnitudes and opposite signs. This is an evidence of transition from low-temperature autoignition to diffusively-supported propagating cool flame.

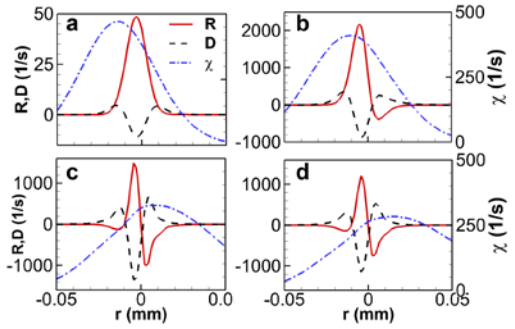

Fig. 4. Evaluation of transport budget for $Y_{CH3OCH2O2}$, the reactive (R) and diffusion (D) terms, and scalar dissipation rate χ. Negative and positive values of distance correspond to the fuel and oxidizer side of the mixing layer. (a) t = 0.04 ms, (b) t = 0.08 ms, (c) t = 0.16 ms, (d) t = 0.2 ms.

After the second stage ignition, the ignition kernels rapidly expand to both richer and leaner mixtures. Propagation in the mixture fraction space can be demonstrated by the conditional averaged parameters against ξ as shown in **Fig. 5**. The conditional HRR is consistent with the instantaneous images shown in **Fig. 2**. The HTC originates around $\xi_{mr,1d}$, and then propagates in both directions to richer and leaner mixtures. On the leaner side the flame front penetrates the ξ_{st} and tribrachial flames are established, as shown in **Fig. 5(a)**. Finally, the lean branch of the edge flame triggers the premixed methane-air flame, which increases the temperature of the premixed mixture at t_4 = 0.41 ms. After the high temperature ignition, the peak temperature increases and moves to leaner mixture fraction and eventually peaks at ξ_{st}, as in **Fig. 5(b)**. Fig. 5(c) shows that methane has been accumulated by the passage of the cool flame. While the second stage ignition occurs in rich mixtures, one branch moves into richer mixtures along with production of methane, where oxygen and other radicals are not sufficient for the combustion of both DME and methane. The other branch propagates into leaner mixtures, where methane is gradually burned and finally totally consumed. In this case, methane is burnt out in lean mixtures but accumulates in rich mixtures, where the conditional methane mass fraction exceeds the original value in the oxidiser stream.

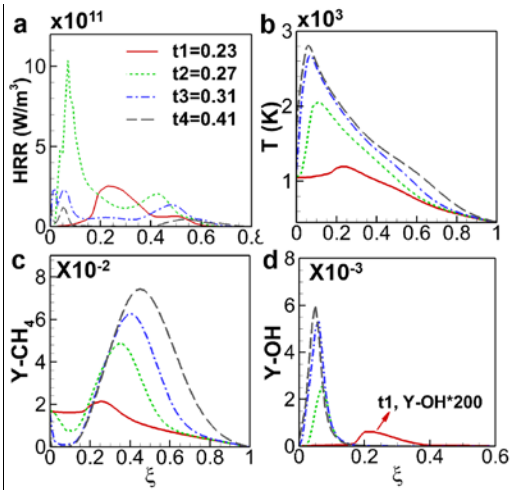

Fig. 5. Conditional averaged (a) heat release rate (HRR), (b) temperature, (c) mass fraction of CH_4, and (d) OH at the indicated time instants (ms).

3.3 Premixed flame initiation

The lean branch of the edge flame gradually initiates the steady propagating premixed methane-air flame. To examine whether the homogeneous premixed methane-air flame has been ignited, the temporal evolutions of $\langle T|\xi=0\rangle$, $\langle HRR|\xi=0\rangle$, $\langle CH4\ RRate|\xi=0\rangle$, $\langle Y_{OH}|\xi=0\rangle$ after the second stage ignition are illustrated in **Fig. 6**, with ξ=0 being defined in the window $0\leqslant\xi\leqslant0.005$. After the premixed flame initiation, these parameters at the premixed flame front (PFF) are recorded, which is demonstrated by $\langle\cdot\,|\xi=0,\ PFF\rangle$. The flame front is limited to the regions with high HRR within the premixed flame thickness. The time required for steady flame propagation can be defined as that for the high HRR flame front appearing in the premixed mixture (which is also consistent with the increase of temperature as shown in **Fig. 6(a)**), which equals 0.32 ms in this case. This is much shorter than the autoignition delay time of the methane-air mixture at the same thermochemical condition, which is 8.24 ms calculated with the homogeneous reactor in the Chemkin software [31]. The HRR and the reaction rate of CH4 as well as Y_{OH} at the propagating premixed methane-air flame front decrease a little until to a stable flame. Note that the equivalence ratio in the initial homogeneous premixed mixture is set to 0.3, and Y_{CH4} is smaller than that accumulated by the partial burning of the DME as shown in **Fig. 5(c)**.

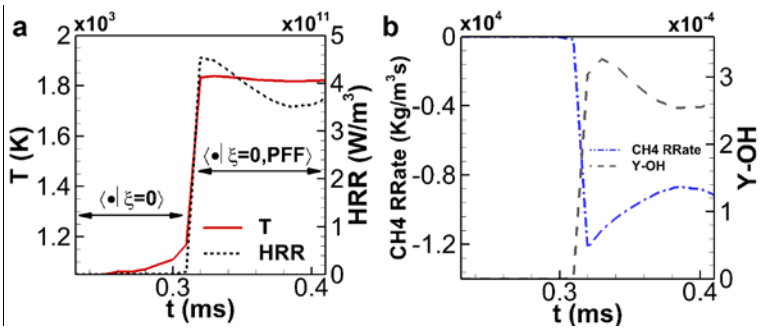

Fig. 6. Temporal evolution of (a) temperature and heat release rate (HRR), (b) CH_4 reaction rate and mass fraction of OH, conditioned on ξ=0 and the premixed methane-air flame front (PFF).

To clarify the characteristics of the combustion waves propagating in the leaner mixture direction after the second stage ignition, temporal evolution of the displacement speed at the flame front is investigated. Here, the displacement speed S_d is defined as:

$$S_d = \frac{1}{\rho|\nabla Y_k|}\left(\dot{\omega}_k - \frac{\partial}{\partial x_j}\left(\rho Y_k V_{j,k}\right)\right)$$

where Y_k, $V_{j,k}$ and $\dot{\omega}_k$ denote the species mass fraction, the species diffusion velocity in the j-direction and the net production rate of species k, respectively. The displacement speed at the flame front S_d is utilized to distinguish between deflagrations and spontaneous ignition fronts. Autoignition is represented by $S_d >> S_L$ occurring at the reaction front, while S_d is comparable with S_L for propagating deflagration. S_L is the laminar flame speed at the same conditions. Here the isocontour of Y_{H2O} that can identify regions of HTC, is chosen to evaluate the displacement speed S_d. The temporal history of S_d (normalized by S_L) and HRR, along with the corresponding ξ at the flame front along line A are plotted in **Fig. 7** and compared with the 1D DNS results. The initial peak S_d is attributed to the thermal run-away in the ignition kernel. Then S_d decreases sharply, which corresponds to the propagation branch to the leaner mixture. The second peak of S_d is attributed to the fierce burning around ξ_{st}, where the HRR increases sharply to extremely peak as in **Fig. 7(b)**. Thereafter, the flame front propagates into lean mixture and eventually into the premixed methane-air mixture. The S_d and HRR decrease gradually, and S_d approaches a steady velocity of 0.2351 m/s, which is consistent with the 1D results. The temporal evolution of S_d indicates a transition between ignition and deflagration modes of combustion at the reaction fronts.

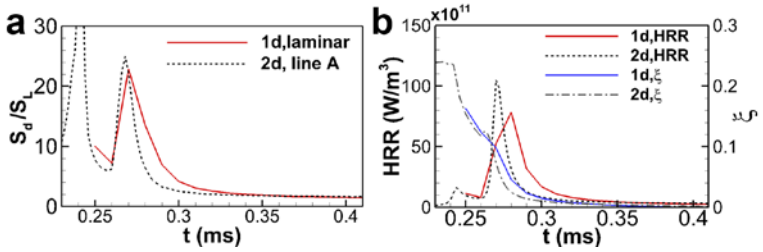

Fig. 7. Temporal evolution of (a) normalized displacement speed S_d, (b) heat release rate (HRR) and mixture fraction ξ at the flame front propagating into leaner mixture after the second stage ignition. Results from 1D simulation are plotted for comparison.

4. Conclusions

Direct numerical simulations are conducted to study the detailed ignition and flame development processes of the turbulent DME/methane-air mixing layer under high pressure conditions relevant to dual-fuel compression-ignition engines. The higher Cetane number DME autoignites and triggers a flame to develop and propagate into the low-Cetane number methane-air homogeneous premixed mixture. The flame initiation dynamics involve low-temperature and high-temperature autoignition, cool flames, propagation and collision of edge flames, and transitions to propagating premixed methane-air flames. The first stage autoignition is initiated around the stoichiometric mixture fraction ξ_{st}, and then the ignition front propagates up the mixture fraction gradient into rich mixtures as a diffusively-supported cool flame. The second stage ignition kernels are spatially distributed in rich mixtures around the most reactive mixture fraction with relatively low scalar dissipation rate χ. The exact locations of kernel formation are important for the overall ignition and stabilization process, and also for the conceptual models of diesel-methane dual fuel combustion.

Results show that triple flames play an essential role during the flame development process. Triple flames are formed and propagate in opposite directions along the ξ_{st} surface, and thereafter they gradually collide with each other and their branches are eventually connected. It is the leading lean premixed branch propagating into the premixed methane-air mixture that initiates the steady propagating methane-air flame. The time required for steady flame propagation is much shorter than the autoignition delay time of the methane-air mixture under the same thermochemical condition. Cool flame and the propagation of triple flames identified in this study are novel features in pilot-ignited

dual fuel combustion, which help to improve our fundamental understanding and have implications for dual-fuel engines. Further investigations are warranted to improve the relevant physical and numerical models as well as the engine performance.

Acknowledgements

This work is supported by the National Natural Science Foundation of China (No. 51576176). Supercomputing time on ARCHER provided under the UK Engineering and Physical Sciences Research Council (EPSRC) projects "UK Consortium on Mesoscale Engineering Sciences (UKCOMES)" (Grant Nos. EP/L00030X/1 and EP/R029598/1) and "High Performance Computing Support for United Kingdom Consortium on Turbulent Reacting Flow (UKCTRF)" (Grant No. EP/K024876/1) is gratefully acknowledged. Tai Jin acknowledges the financial support under the International Postdoctoral Exchange Fellowship Program of the Chinese Scholarship Council (CSC) during his visit at University College London, UK.

References

[1] G.A. Karim, Progress in Energy and Combustion Science 6 (1980) 277-285.

[2] B.B. Sahoo, N. Sahoo, U.K. Saha, Renewable and Sustainable Energy Reviews 13 (2009) 1151-1184.

[3] V. Chintala, K.A. Subramanian, Renewable and Sustainable Energy Reviews 70 (2017) 472-491.

[4] M. Zajadatz, R. Lachner, S. Bernero, C. Motz, P. Flohr, doi:10.1115/GT2007-27730(2007) 559-567.

[5] S.S. Hiremath, S.V. Khandal, N.R. Banapurmath, V.B. Math, V.N. Gaitonde, Fuel 196 (2017) 134-143.

[6] H. Song, C. Liu, F. Li, Z. Wang, X. He, S. Shuai, J. Wang, Fuel 188 (2017) 418-426.

[7] L. Wei, P. Geng, Fuel Processing Technology 142 (2016) 264-278.

[8] J. Sidey, E. Mastorakos, Proceedings of the Combustion Institute 36 (2017) 1721-1727.

[9] S. Schlatter, B. Schneider, Y.M. Wright, K. Boulouchos, Fuel 179 (2016) 339-352.

[10] Z. Wang, J. Abraham, Proceedings of the Combustion Institute 35 (2015) 1041-1048.

[11] E. Demosthenous, G. Borghesi, E. Mastorakos, R.S. Cant, Combustion and Flame 163 (2016) 122-137.

[12] S.L. Johnson, A. Clarke, T. Fletcher, D. Hylands, doi:10.1115/ICEF2012-92133(2012) 781-791.

[13] D.T. Hountalas, R.G. Papagiannakis, A Simulation Model for the Combustion Process of Natural Gas Engines with Pilot Diesel Fuel as an Ignition Source, SAE International, 2001.

[14] I. Taritas, D. Kozarac, M. Sjeric, M. Sierra Aznar, D. Vuilleumier, R. Tatschl, SAE Int. J. Engines 10 (2017) 483-500.

[15] S. Singh, L. Liang, S.-C. Kong, R.D. Reitz, International Journal of Engine Research 7 (2006) 65-75.

[16] E.M. Doran, H. Pitsch, D.J. Cook, Proceedings of the Combustion Institute 34 (2013) 1317-1324.

[17] Y.M.W. Stéphanie Schlatter, Bruno Schneider, Konstantinos Boulouchos, Proceedings of the 7th Dessau Gas Engine Conference, (2011) 293 -307

[18] B.S. Soriano, E.S. Richardson, S. Schlatter, Y.M. Wright, Conditional Moment Closure Modelling for Dual-Fuel Combustion Engines with Pilot-Assisted Compression Ignition, SAE International, 2017.

[19] E. Mastorakos, Proceedings of the Combustion Institute 36 (2017) 2367-2383.

[20] A. Bhagatwala, R. Sankaran, S. Kokjohn, J.H. Chen, Combustion and Flame 162 (2015) 3412-3426.

[21] E. Demosthenous, E. Mastorakos, R. Stewart Cant, Combustion Science and Technology 188 (2016) 542-555.

[22] L.M. Pickett, S. Kook, T.C. Williams, SAE Int. J. Engines 2 (2009) 439-459.

[23] G. Borghesi, E. Mastorakos, R.S. Cant, Combustion and Flame 160 (2013) 1254-1275.

[24] A. Krisman, E.R. Hawkes, M. Talei, A. Bhagatwala, J.H. Chen, Combustion and Flame 172 (2016) 326-341.

[25] A. Krisman, E.R. Hawkes, M. Talei, A. Bhagatwala, J.H. Chen, Proceedings of the Combustion Institute 36 (2017) 3567-3575.

[26] A. Krisman, E.R. Hawkes, J.H. Chen, J Fluid Mech 824 (2017) 5-41.

[27] K. Luo, H. Wang, F. Yi, J. Fan, Energy & Fuels 26 (2012) 6118-6127.

[28] T. Jin, K. Luo, S. Lu, J. Fan, International Journal of Hydrogen Energy 38 (2013) 9886-9896.

[29] U. Burke, K.P. Somers, P. O'Toole, C.M. Zinner, N. Marquet, G. Bourque, E.L. Petersen, W.K. Metcalfe, Z. Serinyel, H.J. Curran, Combustion and Flame 162 (2015) 315-330.

[30] T. Lu, C.K. Law, Combustion and Flame 154 (2008) 761-774.

[31] F.M.R. Robert J. Kee , Ellen Meeks , James A. Miller, CHEMKIN-III: A Fortran Chemical Kinetics Package for the Analysis of Gas Phase Chemical and Plasma Kinetics, Sandia National Laboratories Report 1996.

[32] T. Passot, A. Pouquet, J Fluid Mech 181 (2006) 441-466.

[33] E. Mastorakos, Progress in Energy and Combustion Science 35 (2009) 57-97.

[34] G. Borghesi, A. Krisman, T. Lu, J.H. Chen, Combustion and Flame, doi:10.1016/j.combustflame.2018.02.020(2018).

T. Yao, W. Yang and K. H. Luo, "Direct numerical simulation study of hydrogen/air auto-ignition in turbulent mixing layer at elevated pressures," Computers and Fluids (2018, in press). DOI: https://doi.org/10.1016/j.compfluid.2018.03.075

List of figure captions

Fig. 1. The computational domain with DME and homogeneous methane-air mixture.

Fig. 2. Temporal evolution of heat release rate (W/m^3), the black dashed line is the ξ_{st} surface, the white solid line in (d) is the $\xi_{mr,1d}$ surface, the white solid lines in (f-i) are the ξ=0.005 surface, which approximately demonstrate the premixed methane-air mixture. (g) is a regional zoomed part of (f). The corresponding instants of (a-i) are 0.008, 0.06, 0.16, 0.23, 0.25, 0.29, 0.29, 0.33 and 0.41 ms, respectively.

Fig. 3. Doubly conditioned heat release rate (HRR) on mixture fraction ξ and the indicated scalar dissipation rate range χ, (a) t = 0.06 ms, (b) t = 0.12 ms, (c) t = 0.18 ms, (d) t = 0.22 ms.

Fig. 4. Evaluation of transport budget for $Y_{CH3OCH2O2}$, the reactive (R) and diffusion (D) terms, and scalar dissipation rate χ. Negative and positive values of distance correspond to the fuel and oxidizer side of the mixing layer. (a) t = 0.04 ms, (b) t = 0.08 ms, (c) t = 0.16 ms, (d) t = 0.2 ms.

Fig. 5. Conditional averaged (a) heat release rate (HRR), (b) temperature, (c) mass fraction of CH_4, and (d) OH at the indicated time instants (ms).

Fig. 6. Temporal evolution of (a) temperature and heat release rate (HRR), (b) CH_4 reaction rate and mass fraction of OH, conditioned on ξ=0 and the premixed methane-air flame front (PFF).

Fig. 7. Temporal evolution of (a) normalized displacement speed S_d, (b) heat release rate (HRR) and mixture fraction ξ at the flame front propagating into leaner mixture after the second stage ignition. Results from 1D simulation are plotted for comparison.

List of supplemental material

1. Supplemental materal.docx

This file includes validations of the reduced chemical mechanisms and detailed description of the direct numerical simulation of ignition and flame development in 1D DME/methane-air mixing layer at the same initial thermochemical conditions with the 2D simulations, which is referred in **Section 2 and 3.1** in the main text. Temporal evolution of conditional heat release rate (HRR) during the ignition process, as well as spatial distribution of HRR in the propagating premixed flame are presented. The value of the most reactive mixture fraction for second stage ignition is identified.